Int. J. Solids Structures Vol. 27, No. 11, pp. 1371–1386, 1991
Printed in Great Britain.

0020–7683/91 $3.00 + .00

A NUMERICAL VARIATIONAL METHOD FOR EXTRACTING 3D SINGULARITIES

FARIBORZ GHAHREMANI
Division of Engineering, Brown University, Providence, RI 02912, U.S.A.

(*Received* 1 *November* 1989; *in revised form* 22 *May* 1990)

Abstract—A finite element procedure is developed for calculating the order and mode of singularities at 3D vertices in anisotropic linear elastic solids and composites. It is an extension of the method of Bazant and Estenssoro, although it differs from the latter in some essential aspects. It is based on a variational principle derived from the statement of virtual work on the surface of the unit sphere surrounding the singularity. The sphere is divided into six-node spherical triangles. The singularities of the spherical coordinates at the poles are avoided by coordinate transformations. The three matrices of the quadratic eigenvalue problem are explicitly evaluated and used to advantage. Real and complex eigenvalues and eigenvectors are calculated by inverse treppen iteration. With a relatively small mesh, accuracy is to two decimal places. The method is capable of solving any 3D and any 2D vertex singularity problem with reasonable accuracy and without any assumptions with regard to the behavior of displacements in the neighborhood of line singularities. It is quite robust and stable. Several examples and applications to practical problems are given. A procedure to handle the incompressible case is discussed.

1. INTRODUCTION

Singular asymptotic fields in linear elastic materials have been the subject of several investigations in recent years (Barsoum, 1988; Benthem, 1980; Bazant and Estenssoro, 1979; Somaratna and Ting, 1986; Ting *et al.*, 1985 and references to earlier work contained therein). A short history of the subject is given by Benthem (1979). The general mathematical form of singularities has been studied by Kondrat'ev (1968). For a discussion of topics related to the application of the finite element method to singularities see Strang and Fix (1973).

We briefly review the works relevant to the present study. Our concern is primarily with three-dimensional stress singularities of the form

$$r^{-s}\bar{\sigma}(\theta, \phi; s),$$

where r is the distance from the singular vertex, the tensor $\bar{\sigma}(\theta, \phi; s)$ determines angular variation of the stress; θ and ϕ are the spherical coordinates (see Fig. 1) and s is the order of singularity which can be real or complex. The requirement that the strain-energy should remain finite in the neighborhood of the vertex gives $\mathrm{Re}(s) < \frac{1}{2}$ (in the two-dimensional case $\mathrm{Re}(s) < 1$; Re denotes the real part). For displacements to remain finite, one must have $\mathrm{Re}(s) < 1$.

Using a semi-analytic method, Benthem (1977) was able to calculate s at the vertex of a quarter-infinite crack (Fig. 2a). He created a solution as an infinite series in the Papkovich–Neuber stress functions with unknown coefficients. Every term in the series satisfied the boundary conditions on the crack surface. He satisfied the boundary conditions on the free surface (the xy-plane) by setting the Fourier components of the solution equal to zero on this surface, thereby obtaining an infinite set of equations with zero right-hand sides. From the condition that the determinant of this set (in truncated form) is zero the value of s was calculated. This solution, although very complete, is rather complicated and hard to use. Later (1980) he solved the same problem by the finite difference method. Even though Benthem's results were subsequently verified by others and are believed to be accurate, application of his method to more general problems appears to be difficult.

In an attempt to develop a more general method, Bazant (1974) and Bazant and Estenssoro (1977, 1979) turned to the finite element technique. They formulated a weak

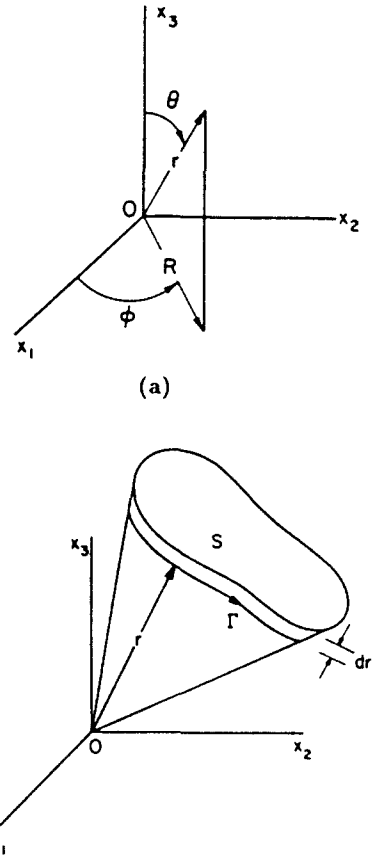

Fig. 1. (a) Spherical coordinates. (b) The cone and the shell.

variational principle for the angular variation of displacements on a unit sphere about the singular point and discretized it by dividing the image of the region on the sphere onto the $\theta\phi$-plane in four-node quadrilateral finite elements. The convergence of their numerical scheme, however, was rather slow; as a result they resorted to extrapolation to obtain accurate answers. Later, Somaratna and Ting (1986) used the same method but with eight-node quadrilateral elements. These latter authors have reported a much faster rate of convergence so that extrapolation was not necessary. They have also extended the method to anisotropic materials.

As will be explained briefly here and becomes clearer in the following sections, Bazant and Estenssoro's procedure suffers from certain shortcomings which make its application to some problems difficult, particularly to situations involving several lines of singularity. By a line of singularity we mean a line every point of which is a singular point, for example the crack front.

The problem of calculating the order of singularity reduces to an eigenvalue problem for s with the eigenfunction represented by displacements or stresses on the unit sphere surrounding the vertex. In discretizing, one can divide into finite elements either the $\theta\phi$-plane or, directly, the surface of the unit sphere. If one divides the $\theta\phi$-plane into uniform quadrilaterals, like Bazant and Estenssoro, the element images on the sphere will be non-uniform regions, where nonuniformity will be greatest at the poles. Consequently, the effectiveness of elements near the poles will be much less than those at the equator. In other words the elements will not be homogeneous. Moreover, all the nodes on the $\theta = 0$ and $\theta = \pi$ lines in the plane will actually represent a single physical point on the sphere. While the approach of Bazant and Estenssoro works for cases with one line singularity, it is not applicable to problems with several such lines, especially when the region of interest contains

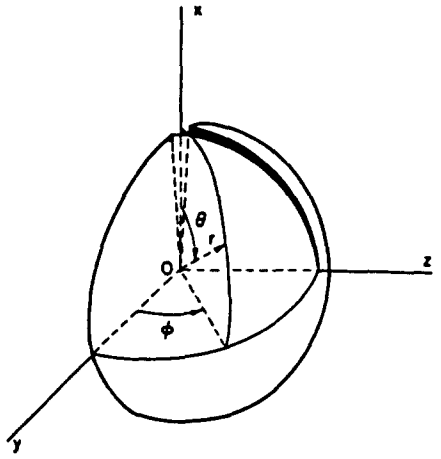

(a)

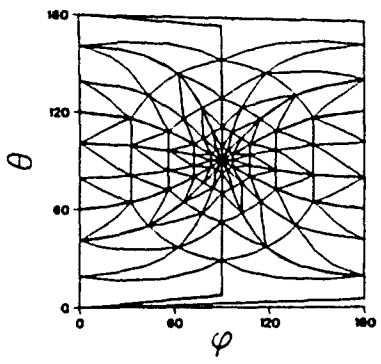

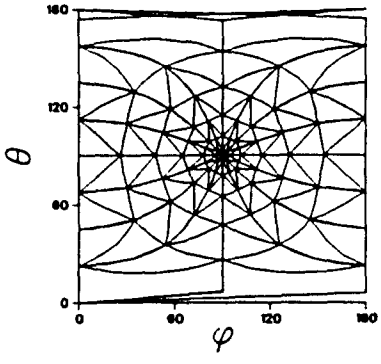

(b) (c)

Fig. 2. (a) Quarter infinite crack. (b, c) Image of finite element grids in the $\theta\phi$-plane.

the poles. (An example of such a complex case is a grain vertex, where several anisotropic crystals with different orientations meet at a point; see Ghahremani *et al.*, 1990). A single line of singularity can be arranged so that it passes through the poles and if it is traction free, it can be treated as a circular with an infinitely small radius. However, this cannot be done in general.

Besides, since the variational principle contains terms like $1/\sin\theta$ which become unbounded at $\theta = 0$, and $\theta = \pi$, for elements containing the poles, accurate numerical integration is difficult. At the poles, the spherical coordinate system itself is singular.

The eigenvalue problem for $\lambda(\equiv 1-s)$ is quadratic, i.e. of the form $(K+\lambda\mathbf{D}+\lambda^2\mathbf{M})\mathbf{x} = 0$, where **K**, **D** and **M** are square, nonsymmetric, banded matrices independent of λ (Bazant and Estenssoro, 1979). None of the authors mentioned seem to have evaluated these matrices explicitly. To calculate λ by an iterative eigenvalue search, it is necessary to repeatedly evaluate $\mathbf{K}+\lambda\mathbf{D}+\lambda^2\mathbf{M}$ for various λ values. Obviously, calculating the matrices **K**, **D** and **M** once and storing them saves a lot of computations.

In our method none of these difficulties arise. We have directly divided the surface of the sphere into elements. This is more natural, but it makes the generation of mesh more

complicated. The mesh generation and refinement is done automatically. To avoid the singularity of the coordinate system at the poles, for every element we have used a local spherical coordinate system in such a way that the center of the element is always close to the point ($\theta = \pi/2$, $\phi = \pi/2$). Then by appropriate transformations, the matrices with respect to a global coordinate system are calculated. Finally, we have separated the above three matrices explicitly. It turns out that it is necessary to decompose only **K**. The three nonsymmetric matrices are stored in banded form. This is the only major storage requirement throughout the computations.

2. BASIC EQUATIONS

In this section we state and prove a variational principle for asymptotic fields at singular points which holds for arbitrary nonlinear and anisotropic materials. It reduces to that of Bazant and Estenssoro (1979) for isotropic elastic materials and to that of Somaratna and Ting (1986) for elastic anisotropic materials.

At the vertex where singularity is expected to exist, we introduce spherical coordinates, as shown in Fig. 1a. Let σ be the stress tensor. We look for values of $\lambda(\equiv 1-s)$ such that separable solutions of the following form can exist

$$\sigma = r^{\lambda-1}\bar{\sigma}(\theta, \phi), \tag{1}$$

where $\bar{\sigma}(\theta, \phi)$ is the stress tensor on the unit sphere, i.e. at $r = 1.0$. In subsequent developments, only the components of the stress tensor on the unit sphere appear. Therefore, for convenience, we drop the bars over $\bar{\sigma}$ and its components.

Let S be a region on the unit sphere and Γ its boundary. Rays emanating from the origin and passing through points on Γ form a cone (Fig. 1b). For the separable stress field (1), the statement of virtual work over the surface S is

$$\int_S \sigma^{ij}\delta\varepsilon_{ij}\,\mathrm{d}S = (2\lambda+1)\int_S T^i\delta u_i\,\mathrm{d}S + \oint_\Gamma T^i\delta u_i\,\mathrm{d}l, \tag{2}$$

for virtual displacement field

$$r^\lambda\delta\mu_i(\theta, \phi). \tag{3}$$

Here $\delta u_i(\theta, \phi)$ is an arbitrary virtual displacement vector on the unit sphere. In the line integral, T^i is the traction vector on the external surface of the cone at $r = 1.0$. The usual summation rule is used for indices $i, j = (1, 2, 3)$. Directions 1, 2 and 3 correspond to arbitrary coordinates. The variations $\delta\varepsilon_{ij}$ are obtained by using (3) in the strain displacement relations for small strains and then putting $r = 1.0$.

The meaning of each term in (2) can be explained as follows: Consider a thin spherical shell of material which occupies the region between r and $r+\mathrm{d}r$ over S, as shown in Fig. 1b. Its edge coincides with the cone mentioned above. If (2) is multiplied by $\mathrm{d}r$, its left-hand side becomes the internal virtual work for this region. On the right-hand side the first term will represent the external virtual work over the top and bottom faces, and the second term that on the edges.

We now prove (2). Let us first introduce the usual notation for the stress components in spherical coordinates

$$[\sigma_{rr} = \sigma_1,\quad \sigma_{\theta\theta} = \sigma_2,\quad \sigma_{\phi\phi} = \sigma_3,\quad \sigma_{\theta\phi} = \sigma_4,\quad \sigma_{r\phi} = \sigma_5,\quad \sigma_{r\theta} = \sigma_6], \tag{4}$$

and analogously for strains, where for example $\varepsilon_{\theta\phi} = \varepsilon_4$ and the engineering definition for $\varepsilon_{\theta\phi}$ is used. Substituting (1) into the equilibrium equations in terms of stresses in spherical coordinates (Love, 1944, p. 91) and canceling $r^{\lambda-2}$, one obtains the three equations of equilibrium in the form

$$\frac{1}{\sin\theta}\frac{\partial\sigma_5}{\partial\phi}+\frac{\partial\sigma_6}{\partial\theta}+(\lambda+1)\sigma_1-\sigma_3-\sigma_2+\sigma_6\cot\theta=0,$$

$$\frac{1}{\sin\theta}\frac{\partial\sigma_4}{\partial\phi}+\frac{\partial\sigma_2}{\partial\theta}+(\lambda+2)\sigma_6+(\sigma_2-\sigma_3)\cot\theta=0,$$

$$\frac{1}{\sin\theta}\frac{\partial\sigma_3}{\partial\phi}+\frac{\partial\sigma_4}{\partial\theta}+(\lambda+2)\sigma_5+2\sigma_4\cot\theta=0. \tag{5}$$

We will use these equations shortly in our proof.

Let the displacements in the r, θ and ϕ directions be u, v and w, respectively. Next, using eqn (3) in the strain–displacement relations (Love, 1944, p. 56) and then setting $r=1$, we get

$$\begin{aligned}
\delta\varepsilon_1 &= \lambda\delta u\\
\delta\varepsilon_2 &= \delta u+\delta v_{,\theta}\\
\delta\varepsilon_3 &= \delta u+\delta v\cot\theta+\frac{\delta w_{,\phi}}{\sin\theta}\\
\delta\varepsilon_4 &= \frac{\delta v_{,\phi}}{\sin\theta}\delta w_{,\theta}-\delta w\cot\theta\\
\delta\varepsilon_5 &= \frac{\delta u_{,\phi}}{\sin\theta}+(\lambda-1)\delta w\\
\delta\varepsilon_6 &= \delta u_{,\theta}+(\lambda-1)\delta v
\end{aligned} \tag{6}$$

where

$$(\ )_{,\theta}=\frac{\partial(\ )}{\partial\theta},\quad (\ )_{,\phi}=\frac{\partial(\ )}{\partial\phi}.$$

The left-hand side of (2) becomes

$$\int_S(\sigma_1\delta\varepsilon_1+\cdots+\sigma_6\delta\varepsilon_6)\,\mathrm{d}S=\int_S\{\sigma_1\lambda\delta u+\cdots+\sigma_6[\delta u_{,\theta}+(\lambda-1)\delta v]\}\,\mathrm{d}S. \tag{7}$$

In this equation, as usual, we use Green's theorem in the $\theta\phi$-plane, transfer the derivatives from δu, δv and δw to the σs, and make use of (5). We get

$$(2\lambda+1)\int_S(\sigma_1\delta u+\sigma_6\delta v+\sigma_5\delta w)\,\mathrm{d}S+\oint_\Gamma(T_r\delta u+T_\theta\delta v+T_\phi\delta w)\,\mathrm{d}l, \tag{8}$$

where, from (4), the coefficients of δu, δv and δw in the surface integral are the traction components on S. The coefficients in the line integral are

$$\begin{aligned}
T_r &= \sigma_6\frac{\mathrm{d}\phi}{\mathrm{d}l}\sin\theta-\sigma_5\frac{\mathrm{d}\theta}{\mathrm{d}l},\\
T_\theta &= \sigma_2\frac{\mathrm{d}\phi}{\mathrm{d}l}\sin\theta-\sigma_4\frac{\mathrm{d}\theta}{\mathrm{d}l},\\
T_\phi &= \sigma_4\frac{\mathrm{d}\phi}{\mathrm{d}l}\sin\theta-\sigma_3\frac{\mathrm{d}\theta}{\mathrm{d}l}.
\end{aligned} \tag{9}$$

It is easily seen that these are the three components of the traction vector acting on the

boundary of the cone at $r = 1.0$. In (9), $\mathrm{d}(\ )/\mathrm{d}l$ is the derivative in the positive direction with respect to the arc-length along Γ (Fig. 1b). Equation (2) is proved.

We give an interpretation of the first term in (8). On the top face of the above thin shell, $\mathrm{d}S = (r+\mathrm{d}r)^2 \sin\theta\,\mathrm{d}\theta\,\mathrm{d}\phi$. From (1), (3) and (4), the external virtual work on this face is

$$(r+\mathrm{d}r)^{2\lambda+1}\int_S (\sigma_1\delta u+\sigma_6\delta v+\sigma_5\delta w)\sin\theta\,\mathrm{d}\theta\,\mathrm{d}\phi.$$

Writing a similar expression for the bottom face with negative sign, setting $r = 1$, adding the two contributions, and keeping only infinitesimals of the first order, one gets the first term of (8) multiplied by $\mathrm{d}r$.

Although in our reasoning we used spherical coordinates, it is obvious that (2) holds in an arbitrary coordinate system. It is also clear that this virtual work statement holds for nonlinear as well as linear materials. For nonlinear materials, in (1) and (5), λ should be replaced by λ', and in (2), 2λ, by $\lambda+\lambda'$. In particular, for power law materials, where $\sigma \propto \varepsilon^n$, $\lambda' - 1 = n(\lambda - 1)$.

3. NUMERICAL RESULTS

A detailed explanation of the discretization of (2) is given in the Appendix. Here we give four numerical examples: (1) the quarter infinite crack in isotropic materials, (2) a transversely isotropic double cone inside an infinite transversely isotropic medium, (3) cracks in laminated orthotropic composites and (4) a rectangular grain vertex, where eight anisotropic crystals meet. In these cases s is real. We only search for the eigenvalues such that $0 < s < 1$. More applications of this method can be found in Ghahremani *et al.* (1990). Many situations involving complex eigenvalues are discussed in Ghahremani and Shih (1990).

3.1. *Quarter infinite crack*

A quarter infinite crack is shown in Fig. 2a. Material is in the half-space $z \geqslant 0$. The crack front is the z-axis; the crack is in the xz-plane; the xy-plane is free. These are an infinite number of eigenvalues and eigenvalues related to rigid body modes which we shall not discuss. We only consider the first two largest eigenvalues, one of which is greater than 0.5, one less. The smaller one corresponds to symmetric displacements with respect to the crack plane and was first calculated by Benthem (1977); the other corresponds to the antisymmetric mode of deformation and was first calculated by Bazant and Estenssoro (1979). Our finite element mesh is shown in Fig. 2b. The region $0 \leqslant \theta \leqslant \pi$, $0 \leqslant \phi \leqslant \pi$ is divided into spherical triangles. Because of symmetry, one can use only half of the mesh which has 513 degrees of freedom. It is found that crowding the elements close to the line singularity increases the accuracy greatly. For the symmetric mode, at $y = 0$, one must set $u_y = 0$, and for the antisymmetric mode $u_x = u_z = 0$. As explained in the Appendix, the traction boundary conditions at the free surface are automatically satisfied.

In Fig. 3, s is plotted against Poisson's ratio ν. Our results, the solid lines, agree with the above-mentioned calculations to within 1%. The values plotted as circles are taken from Benthem (1980).

If one does not take advantage of the symmetry and uses the full mesh, no boundary conditions need be imposed at all. In calculating the displacements, in order to verify that the symmetric and antisymmetric modes actually exist, we used the full mesh and applied no boundary conditions whatsoever. Free surface displacements (at $\phi = 0$) are shown in Fig. 4 for $\nu = 0.3$. They are normalized such that the maximum displacement is unity. For comparison, displacements for plane strain modes I and II and for mode III are plotted. From these, one can conclude that the symmetric mode is very similar to mode I, and the antisymmetric displacement is a mixture of modes II and III. Displacements of points on the

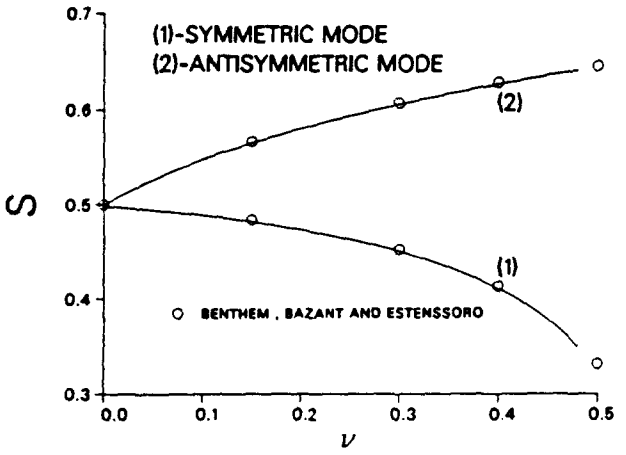

Fig. 3. Order of singularity at the root of a quarter infinite crack as a function of Poisson's ratio.

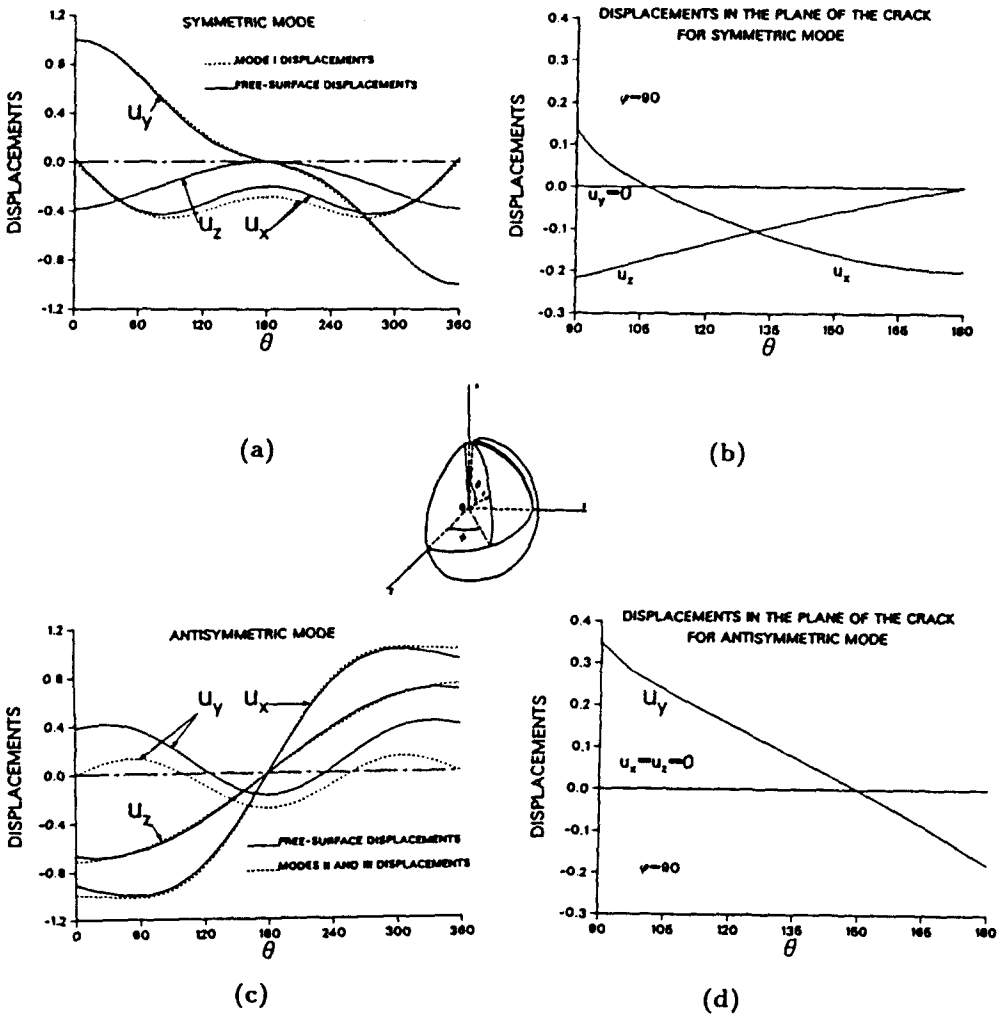

Fig. 4. Displacements for quarter infinite crack ($\nu = 0.3$). Notice that on the free surface, $\phi = 0$; we let θ vary between 0 and 2π.

crack plane (at $\phi = 90^\circ$) are also shown. For the symmetric mode, nonzero displacements at $\theta = 90^\circ$ show that the crack front is deflected upwards and compressed.

At the free surface mode III stresses cannot exist. For $\nu = 0$ the usual plane strain solution satisfies the three-dimensional field equations and boundary conditions. Therefore for $\nu = 0$, we must have $s = 0.5$ exactly. With the mesh shown we obtain $s = 0.499$. Furthermore, the displacements and stresses should be a linear combination of those of modes I and II, with $u_z \equiv 0$. Our results (not shown here) confirm this accurately.

The question of the range of validity of the corner singularity fields has been studied by Nakamura and Parks (1988a,b). For through cracks they have shown that these fields dominate over a distance of about 3% of the thickness of thin plates.

As mentioned earlier, the present method is capable of solving any plane strain singularity problem as well. For example, in Fig. 2a, for $\nu = 0.3$, putting $u_z = 0$ at $\phi = 0$ (to suppress mode III) we calculated $s = 0.50$. The displacements were a linear combination of modes I and II. In order to suppress mode II, we imposed the additional conditions $u_x = 0$ at $(\theta = 0, \phi = 0)$ and at $(\theta = 2\pi, \phi = 0)$. The displacements coincided almost exactly with that of mode I. Then, instead of u_x we set $u_y = 0$ at $(\theta = 0, \phi = 0)$ and $(\theta = 2\pi, \phi = 0)$, and obtained the same eigenvalue but mode II displacements. Inside the material, the largest eigenvalue is $s = 0.5$ with three linearly independent eigenvectors, namely the three modes I, II and III. On the surface, to the first dominant eigenvalue corresponds a single eigenvector, the antisymmetric mode; and to the second eigenvalue, the symmetric.

3.2. *Double cone*

We now turn to anisotropic materials. Consider a transversely isotropic double cone inside an infinite transversely isotropic material, as shown in Fig. 5. The moduli for the cone and the infinite material are the same, but the orientations are different. For the double cone, the axis of material symmetry is oriented along the X_3-axis, while for the medium, at every point it is parallel to the X_1X_2-plane and passes through the X_3-axis. The moduli for transversely isotropic materials can be characterized by five constants $(\alpha, \beta, \gamma, \delta, \varepsilon)$ (Walpole,

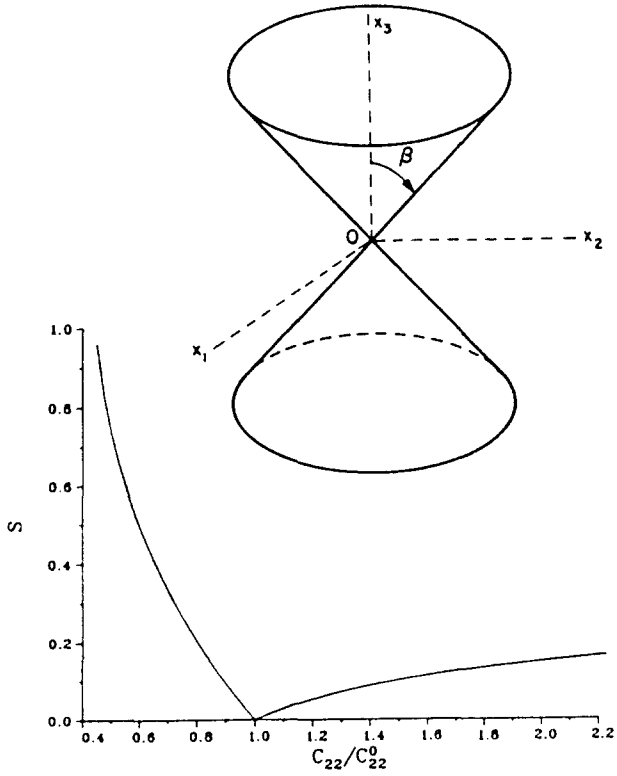

Fig. 5. Singularity order for a transversely isotropic double cone in a transversely isotropic medium.

1969). For Poisson's ratio 0.3 and Young's modulus 1.0, we denote the isotropic moduli by C_{ij}^0 and the constants by $(\alpha_0, \beta_0, \gamma_0, \delta_0, \varepsilon_0)$. Then we vary only α and calculate s. Because of symmetry we analyzed only the region $0 \leqslant \phi \leqslant 5°$. All the nodes with identical z were assigned the same degress of freedom. The displacements in the ϕ-direction were set equal to zero. The results are shown in Fig. 5.

Because of the axial symmetry, this problem can be solved by other completely different methods. This was done, for example, in Ghahremani *et al.* (1990). Since the results of the two analyses were found to be almost entirely identical, we are convinced that the numerical scheme works for anisotropic materials as well.

3.3 *Laminated composites*

The third example was first solved by Somaratna and Ting (1986). It is assumed that a transverse crack is already present at the free surface of a laminated composite (Fig. 6a). The shaded area in the xz-plane represents the crack plane. The crack front is along the z-axis on the interface between the two layers. As in Somaratna and Ting the material of the layers is T300/5208 graphite/epoxy, which is orthotropic. Referred to the material axis, the elastic properties are

$$E_1 = E_2 = 1.54 \times 10^6 \text{ psi},$$
$$E_3 = 22.0 \times 10^6 \text{ psi},$$
$$G_{12} = G_{23} = G_{31} = 0.81 \times 10^6 \text{ psi},$$
$$\nu_{21} = \nu_{31} = \nu_{32} = 0.28$$

where E_i are the Young's moduli, G_{ij}, the shear moduli and ν_{ij}, the Poisson's ratios (Jones, 1975). The orientation of the material axes relative to xyz coordinates is specified by the angle β which is different for the two layers.

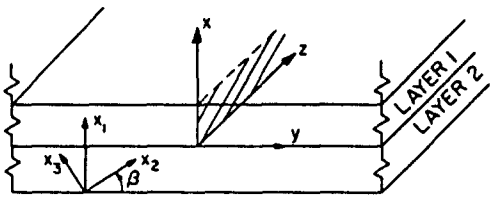

(a)

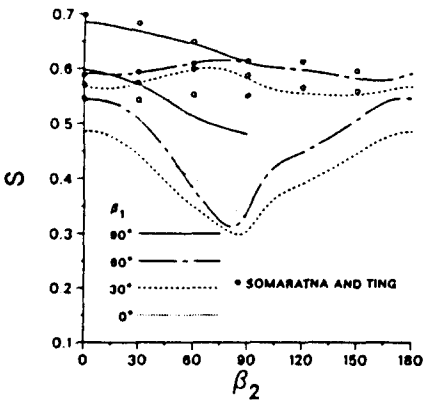

(b)

Fig. 6. (a) Crack in a laminated composite, xy-plane is free. (b) Singularity order.

The finite element grid is shown in Fig. 2c. No boundary condition was imposed at all. Figure 6b shows the first two eigenvalues along with the results of Somaratna and Ting, who calculated only the largest eigenvalue. As in Somaratna and Ting, the strongest singularity occurs at $\beta_1 = 90^\circ$ and $\beta_2 = 0^\circ$. For this case, the free-surface displacements are shown in Fig. 7. Displacements for ($\beta_1 = 90^\circ$, $\beta_2 = 90^\circ$), ($\beta_1 = 0^\circ$, $\beta_2 = 90^\circ$) and ($\beta_1 = 0^\circ$, $\beta_2 = 0^\circ$), which are not presented here, have the larger eigenvalue corresponding to the antisymmetric mode and the smaller one to the symmetric mode. The notable exception is the case shown in Fig. 7 where the larger eigenvalue is associated with the symmetric mode and the smaller one with the antisymmetric mode. For other values of β_1 and β_2 the eigenvectors are neither symmetric nor antisymmetric.

3.4. *Rectangular grain vertex*

In the final example we consider a vertex where eight rectangular grains meet. Figure 8a shows one grain. It is assumed that each grain is a cubic crystal. By taking advantage of symmetry, we analyzed just the region $0 \leqslant \phi \leqslant \pi/4$, $0 \leqslant \theta \leqslant \pi/2$. The [001] direction of the crystal is oriented along the line with direction cosines ($\sqrt{3}/3$, $\sqrt{3}/3$, $\sqrt{3}/3$). The [100] direction is taken to be horizontal. The crystals in the other seven grains are oriented analogously. The symmetry boundary conditions are $w = 0$ at $\phi = 0$ and $\phi = \pi/4$, and

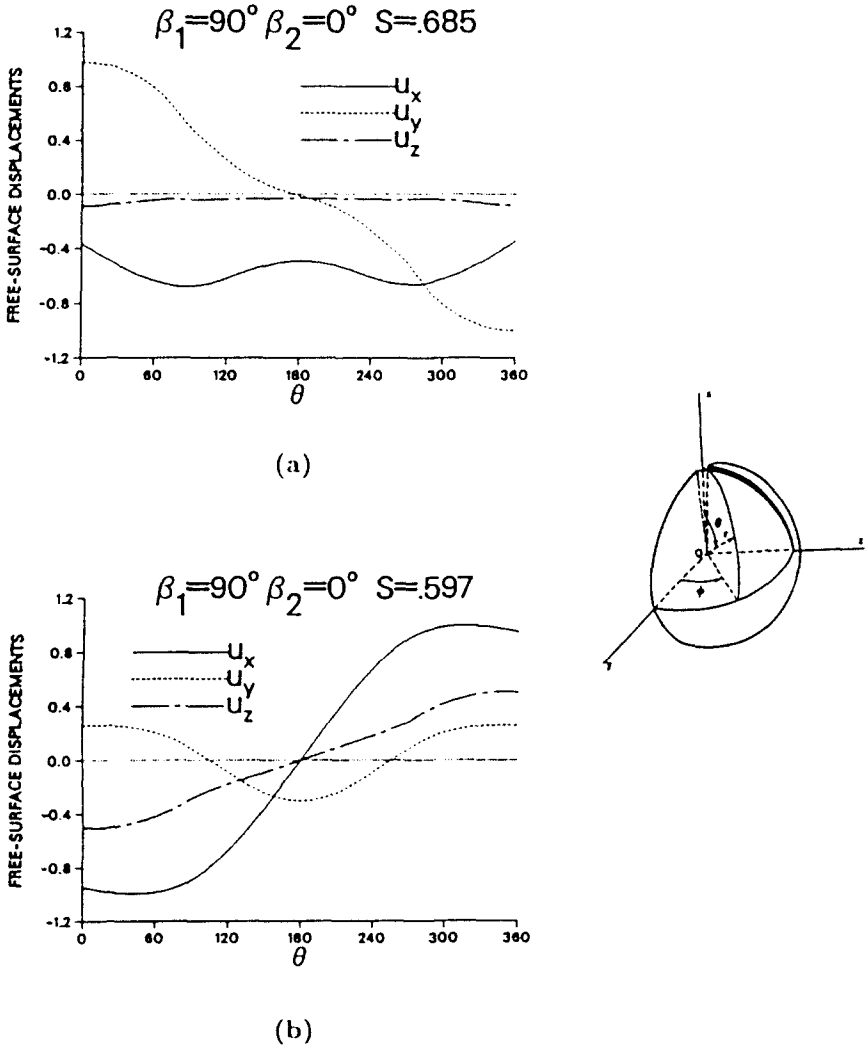

Fig. 7. Free-surface displacements for crack in laminated composite, xy-plane is free. (a) First eigenvalue. (b) Second eigenvalue.

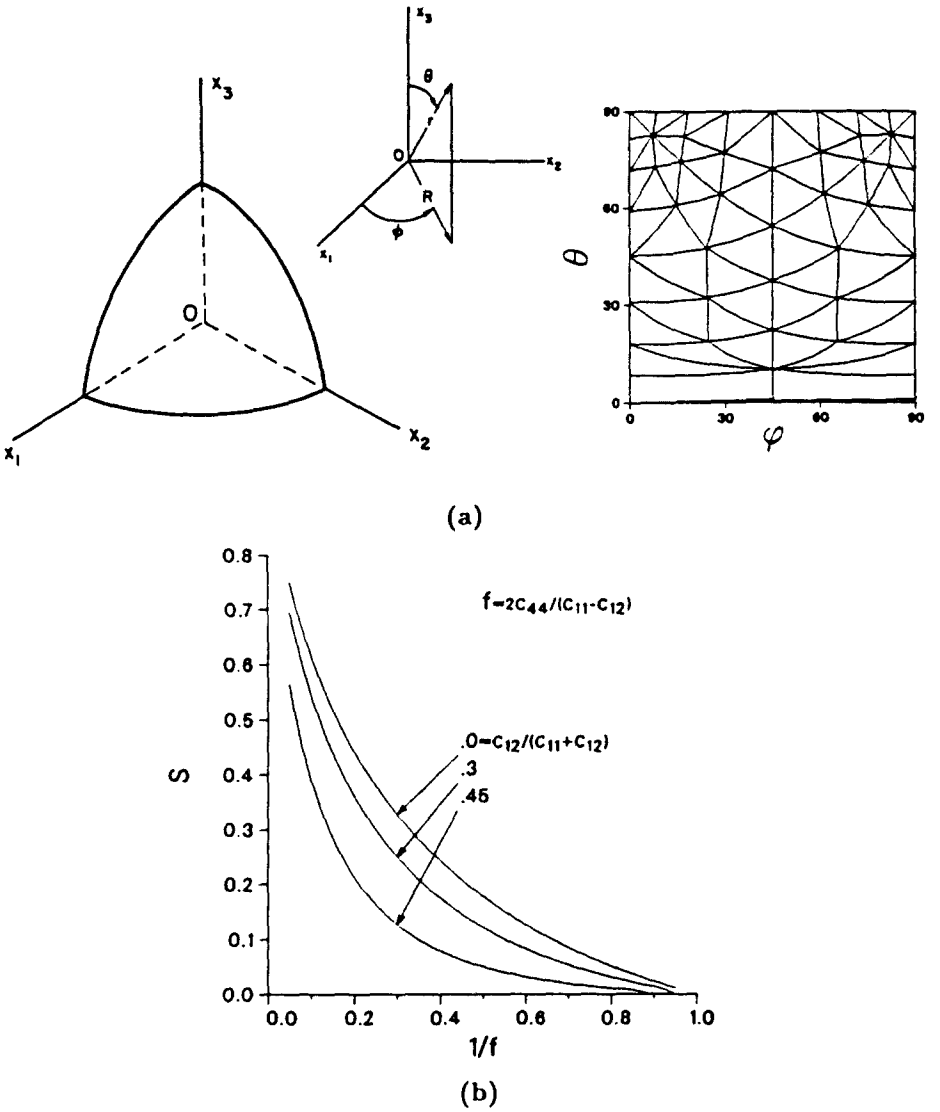

Fig. 8. (a) Rectangular grain vertex where eight cubic crystals join at the origin and the image of the finite element grid on the $\theta\phi$-plane. (b) Order of singularity. Only one grain is shown.

$r = 0$ at $\theta = \pi/2$. For cubic materials, there are two non-dimensional constants, the anisotropy factor $f = 2C_{44}/(C_{11} - C_{12})$ and $\bar{v} = C_{12}/(C_{11} + C_{12})$. The range of f is $(0, \infty)$. When $f = 1$, the material is isotropic. Figure 8b shows the results. For the orientation chosen, the stresses are singular only in the range $1 < f < \infty$. It should be noted that in the most realistic geometry for grain vertex, four grains come to a corner and not eight (Ghahremani *et al.*, 1990).

4. THE INCOMPRESSIBLE CASE

The computer program developed here can be used for values of Poisson's ratio as large as 0.49, but it breaks down for strict incompressibility. We now describe a method for handling this problem which holds for linear and nonlinear incompressible materials.

For small strains, incompressibility requires that the divergence of the displacement field vanishes. For a separable displacement field of the form $r^\lambda u(\theta, \phi)$, $r^\lambda v(\theta, \phi)$, $r^\lambda w(\theta, \phi)$, where u, v and w are the displacements in the r, θ and ϕ directions at $r = 1.0$, setting the divergence equal to zero and solving for u gives

$$u = \frac{-1}{\lambda+2}\left(v_{,\theta} + v\cot\theta + \frac{1}{\sin\theta}w_{,\phi}\right).$$

This equation can be used to eliminate u from the variational principle altogether. Application of this simple technique reduces the number of variables by one, a desirable feature, but in the case of linear materials the resulting eigenvalue problem will be cubic instead of quadratic. This, however, does not pose any difficulty. A method entirely analogous to the one explained in the Appendix for the quadratic eigenvalue problem can be employed. For nonlinear materials, the eigenvalue problem and the equations will be fully nonlinear.

Acknowledgements—During this research, I discussed all matters extensively with Professor John W. Hutchinson of Harvard University. This work was initiated while the author was at Harvard and completed at Brown University. It was supported in part by the National Science Foundation (Grant MSM-88-12779), the Materials Research Laboratory (Grant NSF-DMR-86-14003), the Division of Applied Sciences of Harvard University, Office of Naval Research Grant "Mechanics of Interface Cracks", and Material Research Group at Brown University funded by NSF through Grant DMR 8714665.

REFERENCES

Barsoum, R. S. (1988). Application of the finite element iterative method to the eigenvalue problem of a crack between dissimilar media. *Int. J. Numer. Meth. Engng* **25**, 541–554.

Bazant, Z. P. (1974). Three-dimensional harmonic functions near termination or intersection of gradient singularity lines: a general numerical method. *Int. J. Engng Sci.* **12**, 221–243.

Bazant, Z. P. and Estenssoro, L. F. (1977). General numerical method for three-dimensional singularities in cracked or notched elastic solids. Fracture, *Proc. 4th Int. Conf.* (Edited by D. M. R. Taplin), Vol. 3, pp. 371–385. University of Waterloo, Ontario, Canada.

Bazant, Z. P. and Estenssoro, L. F. (1979). Surface singularity and crack propagation. *Int. J. Solids Structures* **15**, 405–426. See also Erratum (1983), **19**, 661.

Benthem, J. P. (1977). State of stress at the vertex of a quarter-infinite crack in a half-space. *Int. J. Solids Structures* **13**, 479–492.

Benthem, J. P. (1979). On an inversion theorem for conical regions in elasticity theory. *J. Elasticity* **9**, 159–169.

Benthem, J. P. (1980). The quarter-infinite crack in a half-space; alternative and additional solutions. *Int. J. Solids Structures* **16**, 119–130.

Cowper, G. R. (1973). Gaussian quadrature formulas for triangles. *Int. J. Numer. Meth. Engng* **7**, 405–408.

Ghahremani, F. and Shih, C. F. (1990). Corner singularities of three-dimensional planar interface cracks. *J. Appl. Mech.* (in press).

Ghahremani, F., Hutchinson, J. W. and Tvergaard, V. (1990). Three dimensional effects in microcrack nucleation in brittle polycrystals. *J. Am. Ceram. Soc.* **73**, 1548–1554.

Jones, R. M. (1975). *Mechanics of Composite Materials*. McGraw-Hill, New York.

Kondrat'ev, V. A. (1968). Boundary problems for elliptic equations with conical or angular points. *Trans. Moscow Math. Soc.* **17**, 209–292.

Love, A. E. H. (1944). *A Treatise on the Mathematical Theory of Elasticity*, 4th edn. Dover, New York.

Nakamura, T. and Parks, D. M. (1988a). Three-dimensional elastic stress field near the crack front of a thin elastic plate. *J. Appl. Mech.* **55**, 805–813.

Nakamura, T. and Parks, D. M. (1988b). Anti-symmetrical 3D stress field near the crack front of a thin elastic plate. *Int. J. Solids Structures* **25**, 1411–1426.

Parlet, E. N. (Sept. 1984). The software scene in the extraction of eigenvalues from sparse matrices. *SIAM J. Sci. Stat. Comput.* **5**, 590–604.

Somaratna, N. and Ting, T. C. T. (1986). Three-dimensional stress singularities in anisotropic materials and composites. *Int. J. Engng Sci.* **24**, 1115–1134.

Strang, G. and Fix, G. J. (1973). *An Analysis of the Finite Element Method*. Prentice-Hall, Englewood Cliffs, NJ.

Ting, T. C. T. and Hoang, P. H. (1984). Singularities at the tip of a crack normal to the interface of an anisotropic layered composite. *Int. J. Solids Structures* **20**, 439–454.

Ting, T. C. T., Jin, Y. and Chou, S. C. (1985). Eigenfunctions at a singular point in transversely isotropic materials under axisymmetric deformations. *J. Appl. Mech.* **52**, 565–570.

Walpole, L. J. (1969). On the overall elastic moduli of composite materials. *J. Mech. Phys. Solids* **17**, 235–251.

Wilkinson, J. H. (1965). *The Algebraic Eigenvalue Problem*. Oxford University Press, Oxford.

Zienkiewicz, O. Z. (1977). *The Finite Element Method*, 3rd edn. McGraw-Hill, London.

APPENDIX: DISCRETIZATION

Some general remarks about the implementation of the finite element method were made in the Introduction. In this section complete details will be given. We consider linear anisotropic materials. For all the cases considered below, the line integral in (2) vanishes because either the traction vector or the displacements vanish on the boundary of the cone. From (2), the variational principle simply becomes

$$\int_S \Big\{[\sigma_3+\sigma_2-\sigma_1(\lambda+1)]\delta u+\sigma_6\delta u_{,\theta}+\frac{\sigma_5}{\sin\theta}\delta u_{,\phi}+[\sigma_3\cot\theta-(\lambda+2)\sigma_6]\delta v+\sigma_2\delta v_{,\theta}+\frac{\sigma_4}{\sin\theta}\delta v_{,\phi}$$
$$+[-\sigma_4\cot\theta-(\lambda+2)\sigma_5]\delta w+\sigma_4\delta w_{,\theta}+\frac{\sigma}{\sin\theta}\delta w_{,\phi}\Big\}\sin\theta\,d\theta\,d\phi=0. \quad (A1)$$

This equation has terms involving λ^2, λ and no λ. These terms will now be explicitly separated.

From (1) and Hooke's law one can write

$$r^i u(\theta,\phi),\quad r^i v(\theta,\phi),\quad r^i w(\theta,\phi) \quad (A2)$$

for the three displacement components in the r, θ and ϕ directions.

Substituting eqn (A2) into the strain–displacement relations, one gets

$$\varepsilon=\varepsilon^0+\lambda\varepsilon', \quad (A3)$$

where ε^0 and ε' have no λ and

$$\begin{aligned}
\varepsilon_1^0&=0, & \varepsilon_1'&=u,\\
\varepsilon_2^0&=u+v_{,\theta}, & \varepsilon_2'&=0,\\
\varepsilon_3^0&=u+v\cot\theta+\frac{w_{,\phi}}{\sin\theta}, & \varepsilon_3'&=0,\\
\varepsilon_4^0&=\frac{v_{,\phi}}{\sin\theta}+w_{,\theta}-w\cot\theta, & \varepsilon_4'&=0,\\
\varepsilon_5^0&=\frac{u_{,\phi}}{\sin\theta}-w, & \varepsilon_5'&=w,\\
\varepsilon_6^0&=u_{,\theta}-v, & \varepsilon_6'&=v.
\end{aligned} \quad (A4)$$

Let C be the tensor of elastic moduli. From Hooke's law $\sigma=C\varepsilon=C\varepsilon^0+\lambda C\varepsilon'$, therefore,

$$\sigma=\sigma^0+\lambda\sigma', \quad (A5)$$

where

$$\sigma^0=C\varepsilon^0,\quad \sigma'=C\varepsilon'. \quad (A6)$$

Using (A5) in (A1), the principle of virtual work can be written in full

$$\int_S \Big\{[\sigma_3^0+\sigma_2^0-\sigma_1^0+\lambda(\sigma_3'+\sigma_2'-\sigma_1'-\sigma_1')-\lambda^2\sigma_1']\delta u+(\sigma_6^0+\lambda\sigma_6')\delta u_{,\theta}+\frac{\sigma_5^0+\lambda\sigma_5'}{\sin\theta}\delta u_{,\phi}$$
$$+[\sigma_3^0\cot\theta-2\sigma_6^0+\lambda(\sigma_3'\cot\theta-2\sigma_6'-\sigma_6^0)-\lambda^2\sigma_6']\delta v+(\sigma_2^0+\lambda\sigma_2')\delta v_{,\theta}+\frac{\sigma_4^0+\lambda\sigma_4'}{\sin\theta}\delta v_{,\phi}$$
$$+[-\sigma_4^0\cot\theta-2\sigma_5^0+\lambda(-\sigma_4'\cot\theta-2\sigma_5'-\sigma_5^0)-\lambda^2\sigma_5']\delta w+(\sigma_4^0+\lambda\sigma_4')\delta w_{,\theta}+\frac{\sigma_3^0+\lambda\sigma_3'}{\sin\theta}\delta w_{,\phi}\Big\}\sin\theta\,d\theta\,d\phi=0. \quad (A7)$$

We divide the region on the unit sphere into finite elements, spherical triangles with six nodes (Fig. A1a). The sides of the triangle are in most cases great circles, but this is not necessary. When it is convenient, we use triangles with sides that are not great circles. The reasons for choosing this element are: (1) it has been suggested that higher order elements may increase the accuracy (Bazant and Estenssoro, 1979); (2) it is easier to fill a region with triangles; (3) shape functions for these elements are "complete quadratic polynomials" (Zienkiewicz, 1977).

Each element has 18 degrees of freedom (DOFs). For example DOFs 1, 2 and 3 correspond to u, v and w at node one. In terms of the area coordinates L_1, L_2 and L_3, the shape functions are given by (Zienkiewicz, 1977)

$$\begin{aligned}
N^1&=L_1(2L_1-1), & N^4&=4L_2L_3,\\
N^2&=L_2(2L_2-1), & N^5&=4L_1L_3,\\
N^3&=L_3(2L_3-1), & N^6&=4L_1L_2.
\end{aligned} \quad (A8)$$

Using the isoparametric concept and letting $\psi=\phi\sin\theta$, we have

$$\theta=N^i\theta_i,\quad \psi=N^i\psi_i\quad (i=1\text{-}6), \quad (A9)$$

where θ_i and ψ_i are the values of these variables at the nodes. The summation rule for repeated indices is used here and throughout this paper. The reason for using ψ rather than ϕ in (A9) is that, by comparison with known results, it was found that this improves the accuracy.

The displacements inside a triangle are given by

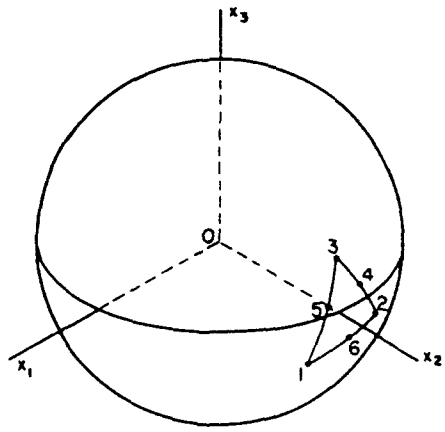

(a)

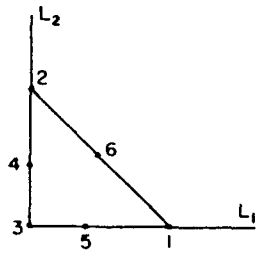

(b)

Fig. A1. (a) An element on the unit sphere. (b) Its image—the standard triangle in L_1L_2-plane.

$$u(\theta,\phi) = U^i(\theta,\phi)x_i$$
$$v(\theta,\phi) = V^i(\theta,\phi)x_i$$
$$w(\theta,\phi) = W^i(\theta,\phi)x_i \tag{A10}$$

where $i = 1$–18, $(U^1 = N^1,\ U^2 = 0,\ U^3 = 0,\ U^4 = N^2, \ldots)$, $(V^1 = 0,\ V^2 = N^1,\ V^3 = 0, \ldots)$, $(W^1 = 0,\ W^2 = 0,\ W^3 = N^1, \ldots)$, $(x_1 = u_1,\ x_2 = v_1,\ x_3 = w_1,\ x_4 = u_2, \ldots)$ and u_i etc. are the nodal displacements. Using (A4) and (A10), we obtain the following expressions for the strain components inside an element

$$\varepsilon_1^i = 0, \qquad \varepsilon_1^r = U^i x_i,$$
$$\varepsilon_2^i = (U^i + V^i_{,\theta})x_i, \qquad \varepsilon_2^r = 0,$$
$$\varepsilon_3^i = \left(U^i + V^i\cot\theta + \frac{W^i_{,\phi}}{\sin\theta}\right)x_i, \qquad \varepsilon_3^r = 0,$$
$$\varepsilon_4^i = \left(\frac{V^i_{,\phi}}{\sin\theta} + W^i_{,\theta} - W^i\cot\theta\right)x_i, \qquad \varepsilon_4^r = 0,$$
$$\varepsilon_5^i = \left(\frac{U^i_{,\phi}}{\sin\theta} - W^i\right)x_i, \qquad \varepsilon_5^r = V^i x_i,$$
$$\varepsilon_6^i = (U^i_{,\theta} - V^i)x_i, \qquad \varepsilon_6^r = W^i x_i, \tag{A11}$$

or written more briefly

$$\varepsilon_i^i = E_{ij}^i(\theta,\phi)x_j, \quad \varepsilon_i^r = E_{ij}^r(\theta,\phi)x_j,$$

where $i = 1$–6, $j = 1$–18 and E_{ij}^i and E_{ij}^r are defined from (A11).

From Hooke's law

$$\sigma_i^r = S_{ij}^r(\theta,\phi)x_j, \quad \sigma_i^i = S_{ij}^i(\theta,\phi)x_j, \tag{A12}$$

in which $i = 1$–6, $j = 1$–18, $S_{ij}^r = C_{ik}E_{kj}^r$ and $S_{ij}^i = C_{ik}E_{kj}^i$. Substituting (A12) and

$$\delta u = U^r(\theta,\phi)\delta x_i, \quad \delta v = V^r(\theta,\phi)\delta x_i, \quad \delta w = W^r(\theta,\phi)\delta x_i,$$

into (A7), we obtain the contribution to virtual work for each element

$$\delta x_i(k_{ij} + \lambda d_{ij} + \lambda^2 m_{ij})x_j, \tag{A13}$$

where

$$k_{ij} = \int_S \left[U^r(S_{1j}^r + S_{2j}^r - S_{1j}^i) + U_{,\theta}^r S_{6j}^r + \frac{U_{,\phi}^r S_{5j}^r}{\sin\theta} + V^r(S_{3j}^r \cot\theta - 2S_{6j}^r) + V_{,\theta}^r S_{2j}^r + \frac{V_{,\phi}^r S_{4j}^r}{\sin\theta} \right.$$
$$\left. + W^r(-S_{4j}^r \cot\theta - 2S_{5j}^r) + W_{,\theta}^r S_{4j}^r + \frac{W_{,\phi}^r S_{5j}^r}{\sin\theta} \right] \sin\theta \, d\theta \, d\phi, \tag{A14}$$

$$d_{ij} = \int_S \left[U^r(S_{1j}^i + S_{2j}^r - S_{1j}^r - S_{1j}^i) + U_{,\theta}^r S_{6j}^i + \frac{U_{,\phi}^r S_{5j}^i}{\sin\theta} + V^r(S_{3j}^i \cot\theta - 2S_{6j}^i - S_{6j}^r) + V_{,\theta}^r S_{2j}^i + \frac{V_{,\phi}^r S_{4j}^i}{\sin\theta} \right.$$
$$\left. + W^r(-S_{4j}^i \cot\theta - 2S_{5j}^i - S_{5j}^r) + W_{,\theta}^r S_{4j}^i + \frac{W_{,\phi}^r S_{5j}^i}{\sin\theta} \right] \sin\theta \, d\theta \, d\phi, \tag{A15}$$

and

$$m_{ij} = \int_S (-U^i S_{1j}^i - V^i S_{6j}^i - W^i S_{5j}^i) \sin\theta \, d\theta \, d\phi, \tag{A16}$$

where $i, j = 1$–18. Finally, assembling these in the usual manner into global matrices, we arrive at the following quadratic eigenvalue problem

$$(\mathbf{K} + \lambda\mathbf{D} + \lambda^2\mathbf{M})\mathbf{x} = 0, \tag{A17}$$

where $\mathbf{K}$, $\mathbf{D}$ and $\mathbf{M}$ are $N \times N$ matrices, N being the total number of DOFs, and $\mathbf{x}$ the N-dimensional vector of nodal displacements.

The integrands in the above expressions for the stiffness matrices of an element contain $1/\sin\theta$ and $\cot\theta$ which become unbounded when θ approaches zero or π. On the other hand, in many applications, the region must contain the poles. To avoid numerical difficulties in calculating the element stiffness matrices we use local coordinates in such a way that the X_2-axis is always perpendicular to the plane passing through the three corners of the element, as is shown in Fig. A1a. The computed matrices are then transformed to a global coordinate system by appropriate rotations. We use Cartesian and cylindrical global coordinate systems. These two options are convenient in applying the boundary conditions. The increase in computer time (because of transformations) is not significant since we assemble the matrices only once, and the major part of computing time is spent on calculating the eigenvalues. The accuracy is also affected little because these rotations involve multiplication by orthogonal matrices, which does not add to the rounding error significantly (Wilkinson, 1965).

In (A13) and (A15) derivatives $U_{,\theta}^r$ etc. appear. To calculate them, one needs to calculate derivatives of the shape functions N^r with respect to θ and ϕ. This is done as follows. From (A8) and (A9), $N^r = N^r(\theta,\psi)$ where $\psi = \phi\sin\theta$. We need to calculate $(\partial N^r/\partial\theta)_{\phi=\text{const}}$, and $(\partial N^r/\partial\phi)_{\theta=\text{const}}$. In can easily be seen that these are given by

$$\left(\frac{\partial N^r}{\partial\theta}\right)_{\phi=\text{const}} = \left(\frac{\partial N^r}{\partial\theta}\right)_{\psi=\text{const}} + \phi\cos\theta\left(\frac{\partial N^r}{\partial\psi}\right)_{\theta=\text{const}},$$
$$\left(\frac{\partial N^r}{\partial\phi}\right)_{\theta=\text{const}} = \sin\theta\left(\frac{\partial N^r}{\partial\psi}\right)_{\theta=\text{const}}$$

Further, from (A8) and (A9), we can calculate $(\partial N^r/\partial\theta)_{\psi=\text{const}}$ and $(\partial N^r/\partial\psi)_{\theta=\text{const}}$ in the standard fashion (Zienkiewicz, 1977).

The integrals are evaluated numerically by Gaussian integration. Equations (A9) map the curvilinear triangle on the sphere into a standard triangle in the L_1L_2-plane, in such a way that the six nodes of the element correspond to the six points on the boundary of the plane triangle as shown in Fig. A1b. At an integration station with coordinates L_1 and L_2 ($L_3 = 1 - L_1 - L_2$), from (A9) we calculate θ and ϕ. All the quantities entering in the integrands in (A14)–(A16) can then be calculated. Notice that in the case of anisotropic materials, the tensor of the elastic moduli must be transformed to spherical coordinates at the point (θ,ϕ) by appropriate rules for the transformation of fourth order tensors. In addition, it can easily be seen that

$$\sin\theta\,\mathrm{d}\theta\,\mathrm{d}\phi = \frac{\partial(\theta,\psi)}{\partial(L_1,L_2)}\,\mathrm{d}L_1\,\mathrm{d}L_2,$$

where $\partial(\theta,\psi)/\partial(L_1,L_2)$ is the Jacobian of θ and ψ with respect to L_1 and L_2. This Jacobian can be calculated easily by using (A9) (Zienkiewicz, 1977). In this way, the integral on the unit sphere is transformed to an integral in the L_1L_2-plane.

Gaussian integration formulas for triangles are given by Cowper (1973). The maximum number of integration points per triangle given there is 13. A 13-point formula integrates a polynomial of degree seven exactly. Although the integrands in our case are not polynomials, they are smooth functions. However, calculation of norms of the matrices in (A17) revealed that the norm of $\mathbf{M}$ is about 1% of that of $\mathbf{K}$ and 10% of the norm of $\mathbf{D}$. This shows that if $\mathbf{M}$ is going to have any effect on the calculations at all, $\mathbf{K}$ must be calculated at least to three significant figures. In view of the limitations on the number of integration points, in order to calculate $\mathbf{K}$ as accurately as desired, one may divide the standard triangle into smaller ones and for each small triangle use 13 or less integration stations. Of course, the number of DOFs will not be affected. In our computations we divided it into four triangles. In principle, within machine tolerance, it is possible to calculate the stiffness matrices as accurately as one wishes.

It can easily be seen that this isoparametric element is not compatible but it becomes so in the limit when the grid is refined indefinitely. It is possible to develop an element which is exactly compatible for this problem. Consider, for example, a spherical triangle with sides that are great circles. Its points can be mapped one-to-one into a plane triangle the three vertices of which coincide with the vertices of the spherical triangle. Points of intersection of a ray through the origin with the two triangles are set in correspondence with one another. This establishes a fully defined one-to-one mapping of the curvilinear triangle into the plane triangle. Now, the area coordinates and the shape functions can be introduced inside the plane triangle in the usual manner. Since in this way, any common boundary of two neighboring elements is mapped one-to-one into the same line, the elements will be compatible. The calculations, however, showed that use of this element does not increase the accuracy. In fact it even decreases it slightly; therefore, we did not use it.

Consider, now, the solution of the quadratic eigenvalue problem (A17). In the existing packages (such as EISPACK for example) there is no program that can handle this problem (Parlet, 1984). We used the following common method to convert the quadratic problem to a linear one (Wilkinson, 1965, p. 633). Let $\mathbf{x}' = \lambda\mathbf{x}$. Equation (A17) becomes

$$\hat{\mathbf{K}}\mathbf{X} = \lambda\hat{\mathbf{D}}\mathbf{X}, \tag{A18}$$

where

$$\mathbf{X} = \begin{pmatrix}\mathbf{x}\\ \mathbf{x}'\end{pmatrix}, \quad \hat{\mathbf{K}} = \begin{pmatrix}\mathbf{0} & \mathbf{I}\\ \mathbf{K} & \mathbf{D}\end{pmatrix}, \quad \hat{\mathbf{D}} = \begin{pmatrix}\mathbf{I} & \mathbf{0}\\ \mathbf{0} & -\mathbf{M}\end{pmatrix} \tag{A19}$$

and $\mathbf{I}$ is the identity matrix. Equation (A18) is now a standard linear eigenvalue problem, but its size is doubled. In practice, however, it is only necessary to store $\mathbf{K}$, $\mathbf{D}$ and $\mathbf{M}$. The inverse of $\hat{\mathbf{K}}$ is

$$\hat{\mathbf{K}}^{-1} = \begin{pmatrix}-\mathbf{K}^{-1}\mathbf{D} & \mathbf{K}^{-1}\\ \mathbf{I} & \mathbf{0}\end{pmatrix}. \tag{A20}$$

Therefore, in using any iterative method of eigenvalue calculation one needs to LU decompose and store only $\mathbf{K}$. For direct iteration, the algorithm we used is described in Wilkinson (1965, p. 604). Since we are interested in calculating the dominant eigenvalue, which is closest to origin, i.e. with the smallest absolute value, we adapted the method to inverse iteration. If the dominant eigenvalue is imaginary, the algorithm gives its real and imaginary parts. The accuracy is to any specified tolerance. The smaller the tolerance, the greater the number of iterations required for convergence. Any inaccuracy in the results has its origin in the discretization finite element approximation.

By shifting the origin of the λ-plane along the real axis, any eigenvalue can be calculated. The closer the shift to the desired eigenvalue, the faster the convergence. For the details of the limitations and peculiarities of this procedure see Wilkinson (1965). For example, if the imaginary part of λ is large, it is difficult to pick it up by our method. However, for most situations of interest, e.g. cracks on bimaterial interfaces, this is not the case and our method will provide an accurate solution.